Best Practice

Comparison of Land Cover Classifications between Ground Observations and Remote Sensing Data in San Diego, California

Sophia Farber[1,*], Peder V. Nelson[2], and Russanne Low[3]

[1] 12th grade, Canyon Crest Academy, San Diego, California, United States of America
[2] Oregon State University; peder.nelson@oregonstate.edu
[3] Institute for Global Environmental Strategies; low.russanne@gmail.com
[*] Corresponding Author: sophiamc.farber@yahoo.com; +1-858-205-0946.

Academic Editor: Jeong Chang Seong

Received: 28 February 2026
Revised: 3 April 2026; 8 April 2026
Accepted: 20 April 2026
Published: 30 April 2026

Abstract: Land cover and its changes are intertwined with human and natural activities. Accurate land cover data is invaluable for land use decisions as well as understanding local and global land cover change. This study explored the local land cover trends of an area of interest in San Diego, California, with the goal of evaluating consistency between ground observations, manual land cover classifications, and land cover maps from remote sensing sources. Ground observations were taken using the Global Learning and Observations to Benefit the Environment (GLOBE) Observer application. Remote sensing sources were accessed through Earth Map, and included the World Cover, Dynamic World, ESRI, and Meta/WRI Global Canopy Height maps of land cover and tree canopy based on satellite imagery. While there was general agreement between ground observations and remote sensing sources over the area as a whole, small inconsistencies were found at nearly all sampling points, and blatant differences were found at three of thirty-seven sampling points between the chosen remote sensing sources as well as between ground observations and remote sensing maps. These inconsistencies were most obvious with the Dynamic World and ESRI datasets, which tended to overgeneralize urban land cover compared to the World Cover dataset. The discrepancies between sources describing the land cover of the same area show the need for caution when examining remote sensing sources and the challenges of remote sensing data, which are increased with differing classification measures.

Keywords: land cover, GLOBE Observer, remote sensing, urbanization, impervious surface

1. Introduction

Remote sensing data are an amazing tool for researchers, leaders, and citizens alike. These data, ranging from satellite images seen on Google Maps to precise measurements of atmospheric conditions, have made studying the Earth from a distance, and thus at a global scale, possible (Gorelick et al., 2017). Land cover studies particularly benefit from remote sensing data because from the satellite view, huge swaths of land can be observed and compared. Regions that may be difficult to reach can be classified with remote sensing data and give scientists a better idea of the land cover in those areas. Satellite imagery is also helpful for land cover classification in that the enormous amounts of data and "zoomed-out" view can help scientists to compare the amounts of different types of land cover more easily than with ground estimates. However, ground observations are critical to validating these remote sensing data.

Satellite images, such as those from the Landsat missions and the images discussed in this study, are taken from a bird's eye perspective, and although there are many remote sensing datasets that create topographical maps and take into account elevation, these images do not. Therefore, while a tree canopy may be clear in a satellite image, its height above the ground is not clear. Additionally, there may be different land cover underneath the tree canopy that is not visible to the satellite. Cloud coverage can also be a barrier to obtaining images of land cover in certain areas. Thus, ground observations, especially those from citizen scientists, can help to validate the land cover observed by satellite images (Low et al., 2021).

The Global Learning and Observations to Benefit the Environment (GLOBE) Observer application is a citizen science application that allows citizens to take and upload photos of the land cover in their area, and

Citation: Farber, S., Nelson, P.V. & Low, R. (2026). Comparison of Land Cover Classifications Between Ground Observations and Remote Sensing Data in San Diego, California. Journal of Earth Observation and Geospatial Applications, 2(1), 59–68. https://doi.org/10.65372/hgazje62

upload them to the GLOBE Visualization System, where they can be accessed openly (NASA, 2025). The benefit of a citizen science approach to ground observation collection is that citizen scientists are located globally, and can provide more data, faster, from many locations (Nelson et al., 2024).

The purpose of this study is to qualitatively explore the accuracy of ground observations compared to remote sensing data for the selected area of interest (AOI), located in San Diego, California. First, ground observations were made using the GLOBE Observer application to show the feasibility of citizen science contributions to land cover research (Nelson et al., 2024). Then, manual classifications of land cover were made using the Collect Earth Online (CEO) platform (Saah et al., 2019) at the same locations in order to provide a verified dataset of the land cover. Finally, land cover classifications from several remote sensing sources were compared with the CEO data and ground observations to reveal consistencies and discrepancies between the data. To provide context for the area of interest, historical land cover data were collected from the Annual National Land Cover Database (Jin et al., 2023; USGS, 2024).

Providing an example of the repeatable process of comparison of ground observations and remote sensing data, this study supports further improvement of land cover classifications based on remote sensing data. The discrepancies found between remote sensing data and manual classifications also demonstrate the need for extra consideration of remote sensing data when it is used for land use decisions because of the differences between remote sensing datasets, classification approaches, and land cover examination strategies over the same area.

2. Study Area and Methods

2.1. Study Area

The study area consisted of a 3 km × 3 km AOI in San Diego, California (Figure 1). The City of San Diego is located in the Southwest corner of the continental United States, framed by the Pacific Ocean to the west and deserts and mountains to the east. Topographic features are diverse, ranging from coastal bluffs, estuaries, and lagoons, to mountains, mesas, and canyons. Similar to much of Southern California, the most common natural disasters are earthquakes and wildfires, however San Diego's location on the coast also puts the city at risk of tsunamis. The coastal desert climate keeps temperatures consistent in the low twenties Celsius, along with consistently little rainfall (U.S. Federal Government, 2025). San Diego regularly sees a marine layer—a layer of cloud or fog that forms over the ocean and coast due to water that is colder than the air above it—in the mornings, especially in early summer (NOAA, 2023).

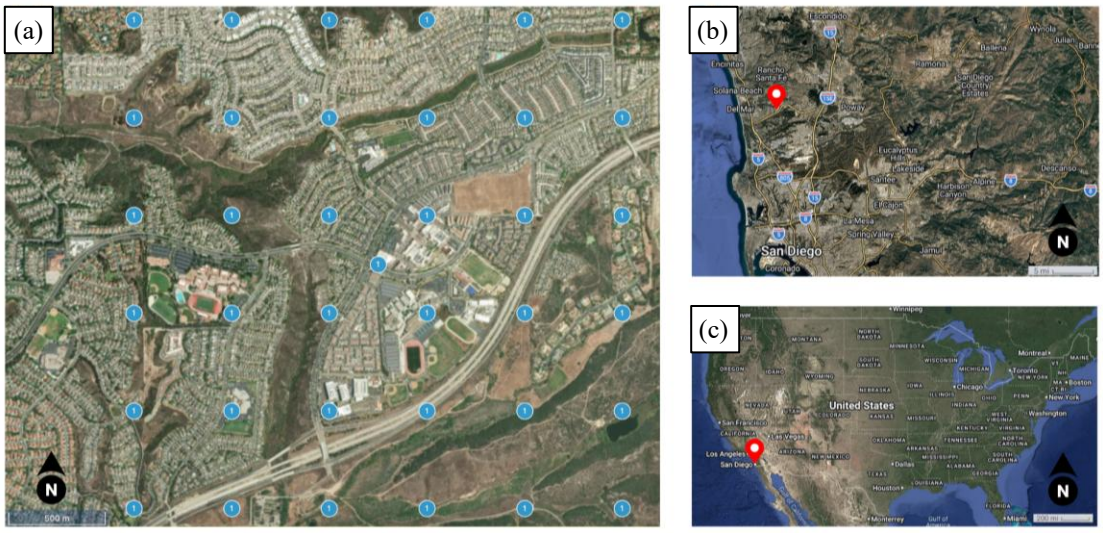

Figure 1. (a) Study area as viewed on the Collect Earth Online platform. Blue pins show the locations of each of the 37 data sites in the AOI, with the number 1 inside each point indicating one data site at the point. (b) Location of study area in California, as viewed with Google Maps. (c) Location of study area in the United States, as viewed with Google Maps.

San Diego is known globally for features ranging from the San Diego Zoo to significant military installations, including Naval and Marine Corps bases. San Diego is also a hotspot for innovative industries including biotechnology, software, and Smart City technology. The center of the study area is located around 35 miles north of the San Ysidro Border Crossing with Mexico. With 1.4 million people, the City of San Diego is the second most populous city in California, and eighth most populous in the United States. San Diego is also an incredibly multicultural city.

The AOI was centered around the Pacific Highlands Ranch community, with the California State Route 56 highway running diagonally through it in the southwest to northeast direction. Deer Canyon in the southeast corner and Gonzales Canyon in the northwest corner place the suburban area in between two natural spaces. The center portion of the AOI has rapidly urbanized within the last three decades, with construction of a majority of suburban housing developments, several apartment and condo complexes, schools, and a central shopping center appearing within the last twenty years. This rapid human development makes the AOI of use in evaluating inconsistencies between remote sensing and ground-based observations over a period of rapid change in land cover. The majority of data collection sites within the AOI consisted of built-up land, with the canyons preserving wild space.

2.2. Data

The AOI was a 3 km × 3 km area, following the Adopt a Pixel 3 km method (Low et al., 2021). The data collected consist of images at 37 points, as will be further discussed in Section 2.3: Methods, within the AOI and images of the entire AOI over a longer time period. Ground observations consisted of photos taken with the GLOBE Observer application at each of the 37 points selected within the AOI. Limitations of the ground observations came in the form of inaccessibility of exact observation sites due to private property lines and obstructive vegetation. Remote sensing sources were accessed from the Earth Map website, with the following land cover and forestry layers used: Meta/WRI Global Canopy Height (Tolan et al., 2024), World Cover 10 m (Zanaga et al., 2021), Dynamic World (Brown et al., 2022), and ESRI 2017/2024 (Karra et al., 2021). The Meta/WRI Global Canopy Height maps global tree canopy height using data from Worldview-4. World Cover 10 m is a global land cover map created with Sentinel-1 and Sentinel-2 imagery at a spatial resolution of 10 m. Dynamic World and ESRI 2017/2024 have 10 m spatial resolution and are land classification datasets based on Sentinel-2 imagery. Additionally, manual land cover classifications were made through the CEO platform (Saah et al., 2019) for the 37 data sites in the AOI. CEO classifications were made with the Mapbox Satellite base imagery, which combines several remote sensing sources to create a global layer at 1−2m spatial resolution, with higher resolution available in select locations (Saah et al., 2019; Mapbox, n.d.).

To analyze land cover change over time, two sets of image chips were compared over a 40 year period to evaluate the entire AOI area. First, annual satellite images at 30 m spatial resolution from the Landsat missions were collected through the Google Earth Engine Landsat time series (LTS) Explorer (Braaten, n.d.). These image chips cover the entire 3 km × 3 km area and utilize SWIR1/NIR/GREEN for the RGB Visualization, which assigns the red channel to Shortwave Infrared 1, green channel to Near Infrared, and blue channel to Green visible light, creating a vibrant false color composite to highlight changes in vegetation health and greater contrast between land cover elements. Second, fractional impervious surface images from the Multi-Resolution Land Characteristics (MRLC) Consortium Annual National Land Cover Database (Jin et al., 2023; MRLC Consortium, n.d.) were used. The fractional impervious surface images use a 30 m resolution based on Landsat data (USGS, 2024), thus making the LTS and MRLC data consistent in spatial resolution for comparison.

2.3. Methods

37 points within the AOI were generated in a 6 × 6 grid pattern with an additional center point, called the centroid. Each of the 36 non-centroid points is spaced 500 meters from its adjacent points, and is placed in the center of a 10000 m² (100 m × 100 m) area. The points were numbered starting with 1 in the bottom left corner, and increasing up each column of the grid, with increasing columns from left to right (Figure 2). The centroid was considered to be point 0. The coordinates for each point were stored in a CSV file, while a GeoJSON file was used to store the boundaries of the AOI, the boundaries of the 10000 m² boxes around each point, and the coordinates of each point.

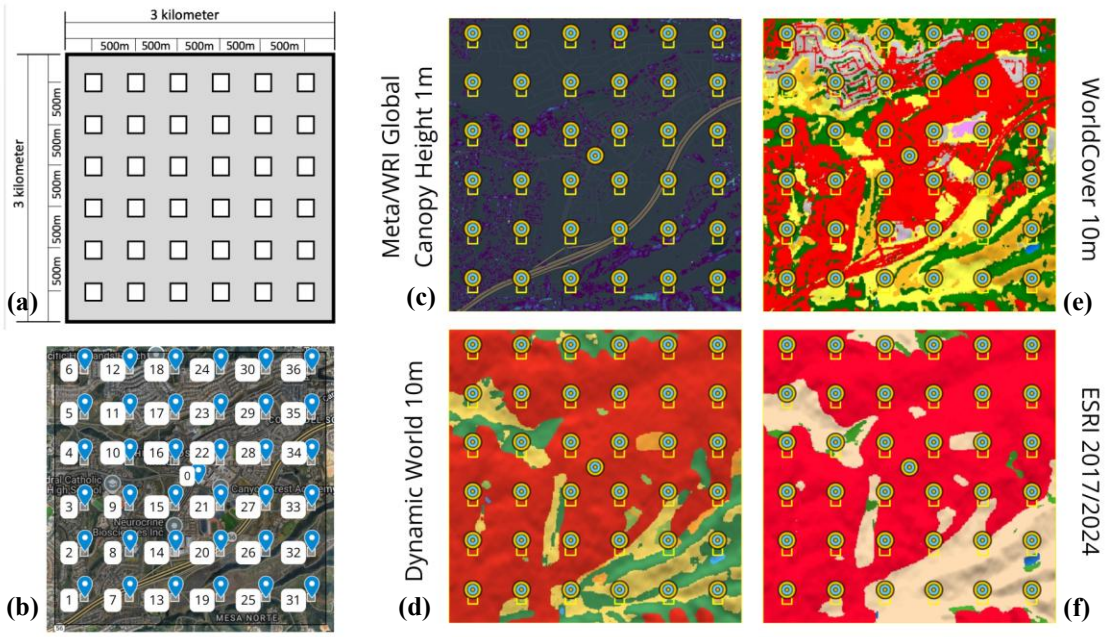

Figure 2. (a) Adopt a Pixel 3 km framework used to create an AOI (Source: Peder Nelson). (b) Numbered sampling points in AOI grid. (c–f) AOI as viewed on Earth Map with land cover and tree canopy layers; (c) Meta/WRI Global Canopy Height 1 m. (d) Dynamic World 10 m. (e) World Cover 10 m. (f) ESRI 2017/2024. All show land cover classifications that are different in some areas.

Of the 37 points, ground observations using the GLOBE Observer application were captured within the 10000 m² area at 34 points. Data were collected for the inaccessible points (33, 34, 36) slightly outside of the designated area and thus are not representative of the land cover at the point but are similar. Each ground observation included six photos: one in each of the cardinal directions, one down toward the ground, and one up towards the sky. These photos were uploaded to the GLOBE Visualization System.

At each of the 37 points, eight image chips from the Earth Map website were collected. These eight images included: one image of the 10000 m² area surrounding the point of each of the four Earth Map layers (Meta/WRI Global Canopy Height, World Cover 10 m, Dynamic World, and ESRI 2017/2024), one graph of the area distribution of tree canopy heights within the 10000 m² area from the Meta/WRI Global Canopy Height dataset, one graph of the historical distribution of land cover categories from 2020 to 2021 of the World Cover 10 m dataset, one graph of the historical distribution of land cover categories from 2016 to 2024 of the Dynamic World 10 m dataset, and one graph of the historical distribution of land cover categories from 2017 to 2023 of the ESRI 2017/2024 dataset. The image chips of the 10000 m² area surrounding each point, from each of the Earth Map layers, were chosen to use the most recent data available from each respective layer. The most recent Meta/WRI Global Canopy Height data is from 2020, the most recent World Cover 10 m layer is from 2021, and the most recent Dynamic World 10 m and ESRI 2017/2024 layers are from 2024.

Additionally, a graph generated by the LTS of the Normalized Burn Ratio (NBR) from 1984 to 2025 was included for each point. Normalized Burn Ratio values provide insight into the vegetation characteristics of an area, as lower NBR values indicate less vegetation and recent burns, while higher NBR values indicate healthy and thicker vegetation.

At each of the 37 points, manual land cover classifications were made with CEO. Each point was divided into 100 subpoints, with each subpoint classified into one of the following thirteen categories: Trees_CanopyCover, Shadow, Bush/Scrub, Unknown, Grass, Bare Ground, Cultivated Vegetation, Building, Water > Lake/Ponded/Container, Water > Rivers/Stream, Water > Irrigation Ditch, Impervious Surface, Wetlands. An image of the 100 color-coded classifications, in a 10 × 10 grid overlaid onto the 10000 m² area, was then compared to the land cover classification maps from Earth Map. These manual classifications provided an additional land cover layer to compare with the ground observations and land cover maps from Earth Map.

Finally, as stated earlier, annual satellite images of the 3 km × 3 km area were used to compare land cover over a longer period of time. Evaluating change over time in land cover was desired in order to reveal the overall trends that may have led to inconsistencies between ground observations and the remote-sensing-based land cover classification layers from Earth Map. These images revealed the rapid urbanization of the entire AOI over the twenty years between 2004 and 2024. A total of 42 images from the LTS collection correspond to the years 1984 to 2025, and 40 fractional impervious surface images from the MRLC database correspond to the years 1985 to 2024.

To quantify the overall built-up area for the entire 3km by 3km AOI, a geospatial analysis was performed in QGIS. For the MRLC fractional impervious surface data, the Zonal Statistics tool was used to calculate the mean pixel value across the AOI, which represents the total percentage of impervious surface cover. For the land cover classification layers (World Cover 10 m, Dynamic World 10 m, and ESRI), the area of the "Built-up" or "Built Area" classification was calculated as a percentage of the total 3 km × 3 km area. These calculations were performed using the 2024 layers for ESRI and Dynamic World, and the 2021 layer for World Cover. The area value for built-up classification values for each remote sensing source was found using the Change Matrix values from the Earth Map Analytics tool for the 3 km × 3 km boundary. For the CEO classifications, at each of the 37 data sites, the number of "Impervious Surface" and "Building" classifications were counted out of the 100 classifications made at the site. The total number of "Impervious Surface" and "Building" classifications were then summed. The total percentage of impervious surface cover for the AOI using CEO data was then calculated by dividing the aforementioned sum by the total number of land cover classifications made using CEO, which was 3700 classifications (100 classifications per data site).

2.4. Thematic Consistency Challenges and Qualitative Approach

Due to the lack of consistent land cover classification categories between the remote sensing sources, as well as the visual nature of the data, a contingency table for this study was not possible. A prime example of the similar but inconsistent descriptions of land cover elements is the categories provided by the Earth Map land cover layers. World Cover 10 m uses "grassland" and "shrubland" labels, while ESRI uses "rangeland" and "crops," and Dynamic World uses "grass" and "shrub & scrub." The majority of data collected for this study comes in the form of images, with the different land cover layers, satellite images, and manual photo sources providing varying numbers of pixels for the same area. Therefore, a complete statistical analysis was deemed unfeasible and the accuracy assessment is mainly qualitative rather than quantitative.

3. Results

3.1. Land Cover Change over Time and Fractional Impervious Surface in the AOI

Land cover change over time in the AOI was analyzed via comparison of the LTS images from 1984 to 2025, and the MRLC fractional impervious surface images from 1985 to 2024. These sets of images were highly consistent with each other (Figure 3). Starting in the 1980s, the coloration of the AOI was pink and red according to the LTS images, showing dirt and land without any buildings. This pink color is exaggerated by the RGB Visualization. A thin line of impervious surface crossed the center of the AOI as shown in the MRLC images. These shapes and colors remained consistent, with minimal growth of impervious surface, until 2003. 2003 shows a larger increase in impervious surface, and the following year, 2004, a substantial increase in impervious surface and transformation of the area is seen in the LTS image. Before 2003, it can be inferred that less than a quarter of the area was impervious surface, while in 2004, it can be inferred that only about a quarter of the area was not impervious surface. In the 21 years since this disruption, fractional impervious surface continued to increase slowly, with the final image in 2024 showing only the southeast corner of the AOI and a small portion of the northwest corner of the AOI not covered by impervious surface. These areas correspond to Deer and Gonzales Canyon as mentioned in Section 2.1. The LTS images show after the year 2004 a drastic change from the dominant red color before the disruption to a mix of dark green, purple, brown, and white, showing the colors of the urbanization of the area, with the building of a suburban neighborhood with schools, houses, roads, and a shopping center.

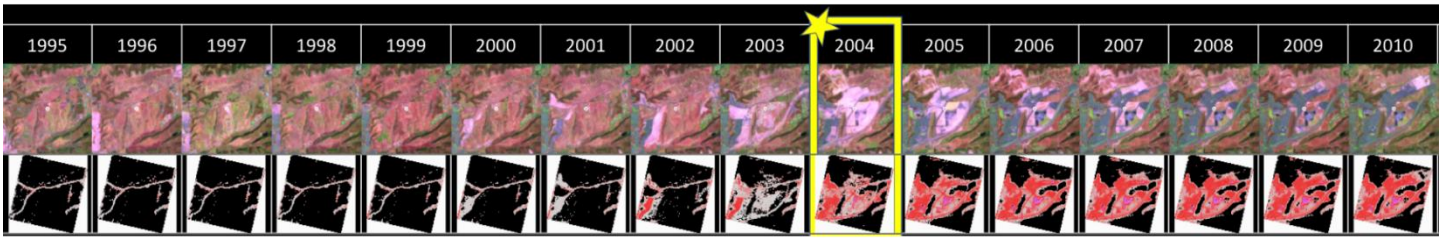

Figure 3. Comparison of annual LTS and MRLC fractional impervious surface images of the AOI from 1995 to 2010, showing the year 2004, when land cover rapidly changed. The top row shows LTS images, and the bottom row shows MRLC fractional impervious surface images.

These visual observations are confirmed by quantitative analysis of the MRLC images. From 1985 to 2001, the percentage of fractional impervious surface in the AOI remained under two percent. In 2002, this figure jumped to 4.58%, in 2003 the percentage increased to 6.22%, and in 2004, a significant increase resulting in 17.12% impervious surface. This number steadily rose to 38.82% fractional impervious surface in 2024 (see complete annual data in Zenodo repository).

The land cover layers from Earth Map, while differing in labeling schemes (as will be further explained in the Discussion section), consistently included a label for built-up areas, which we made to correspond to impervious surface as the other land cover category labels would not be considered impervious surface. To represent the most recent extent of urbanization in the AOI, built-up area percentages were calculated using the latest available data layers from each source: 2024 for ESRI and Dynamic World 10 m, and 2021 for World Cover 10 m. The manual classifications from CEO can also be used to estimate the total impervious surface in the AOI, as the manual classifications from each of the 37 points would be expected to be representative of the AOI as a whole. The total impervious surface was considered to include both the "Impervious Surface" and "Building" labels from CEO. These results, along with the MRLC 2024 fractional impervious surface value, are shown in Table 1.

While the MRLC, CEO, and World Cover 10 m data returned similar percentages of fractional impervious surface, Dynamic World 10 m and ESRI were about 30 percentage points higher. Although Dynamic World 10 m and ESRI are close to each other, within 2 percentage points, their values are far from the other three sources.

Table 1. Fractional Impervious Surface in 3 km × 3 km AOI according to remote sensing sources. The "Land Cover Category" refers to the label for impervious surface that each remote sensing source uses.

Dataset	Land Cover Label	Percent Fractional Impervious Surface
World Cover 10 m	Built-up	41.08%
Dynamic World 10 m	Built Area	69.53%
ESRI 10 m	Built Area	71.11%
MRLC	Fractional Impervious Surface	38.82%
CEO	Impervious Surface; Building	37.43%

3.2. Comparison of Land Cover Classifications at Sampling Points

At 34 of the 37 sampling points, remote sensing datasets predominantly matched GLOBE Observer ground observations and manual classifications from CEO. This "predominant" matching is assessed through visual confirmation due to the aforementioned unfeasible contingency table (for the complete table of all 37 sampling points and their associated remote sensing image chips, ground observations, and CEO manual classifications, see the poster in the Zenodo repository). Although at no data site there was 100% agreement between CEO classifications and a remote sensing land cover dataset, there were several sites with near perfect matches (Figure 4). The only 100% agreement between a remote sensing source and CEO classifications was the absence of trees shown in both CEO classifications and the Meta/WRI Tree Canopy layer, such as at points 7, and 27 (see Figure 4, indicated by green checkmarks in the Tree Canopy column). Vegetation and built-up areas were accounted for in the same or recognizably similar proportions in the remote sensing data when compared to the CEO data. However, at three points, 18, 27, and 33, remote sensing sources conflicted with each other as well as with field observations or CEO data, as indicated by the red "x" mark symbols in Figure 4.

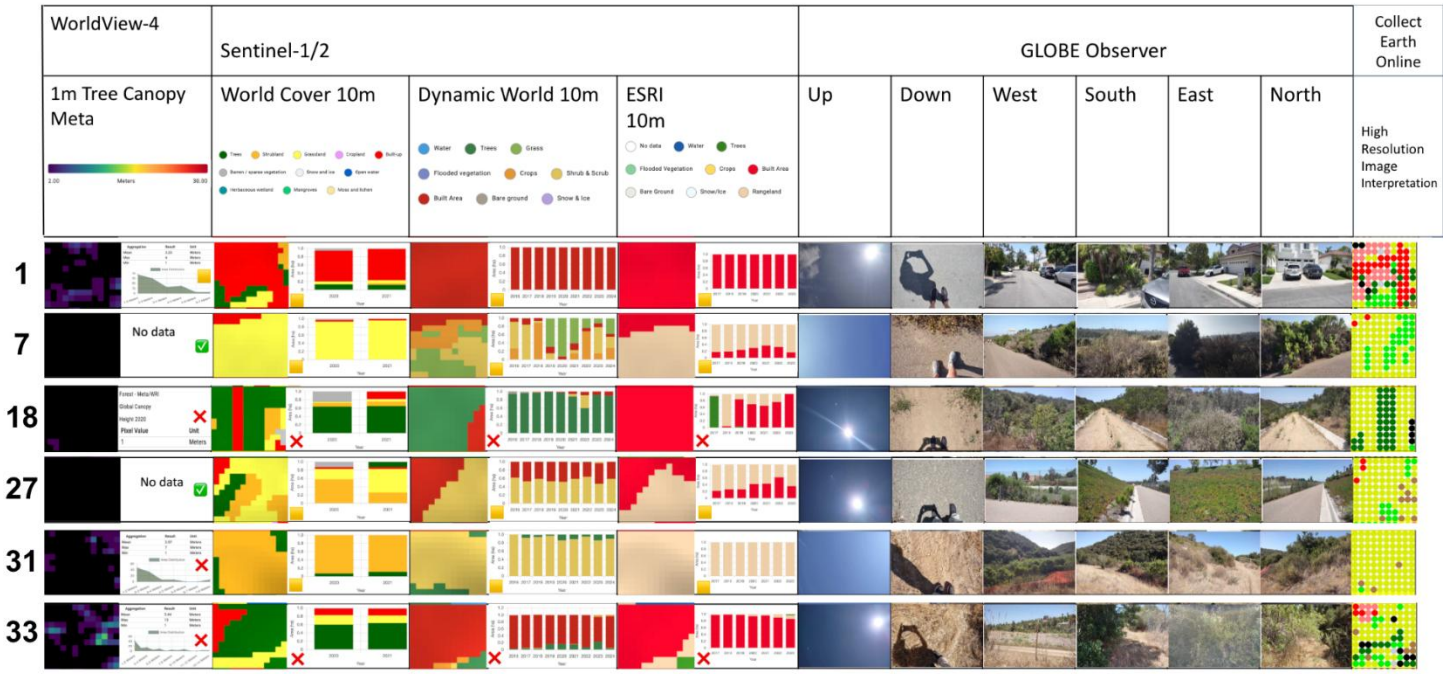

Figure 4. A sample of several data sites within the AOI where the many remote sensing sources, ground observations, and CEO manual classifications are compared. The sampling point number is on the far left. The source of the remote sensing data is listed in the top row, with the name of the dataset and key to its color code. Generally the color code of the land cover classifications is consistent with broad categories, with all 3 land cover maps and CEO classifications using red for impervious surface, dark green for trees, and yellow/orange/tan for an interpretation of grass/shrub/scrub/bush/rangeland/cropland. The data sources in the table listed from left to right are as follows: Meta/WRI Global Canopy Height 1 m image chip, Meta/WRI Global Canopy Height area distribution graph, World Cover 10 m image chip, World Cover 10 m historical distribution of land cover categories from 2020 to 2021, Dynamic World 10 m image chip, Dynamic World 10 m historical distribution of land cover categories from 2016 to 2024, ESRI 10 m image chip, ESRI 10 m historical distribution of land cover categories from 2017 to 2023, GLOBE Observer ground observations, CEO manual land cover classification grid. Sampling points 1, 7, and 31 show consistency between sources, while sampling points 18, 27, and 33 show inconsistent land cover classifications between remote sensing sources and with the ground observations and CEO classifications.

At point 18, ground observations showed a dirt trail surrounded by tall brush and small trees. Vegetation was thick and abundant around the trail. When the ground observations and CEO manual classifications did not match any of the remote sensing sources, this point highlighted a serious discrepancy among the sources of data. The Meta/WRI Global Canopy Height data gave a value of zero canopy height in the entire 10000 m² area, clearly contradicted by the trees in the photos. The World Cover 10 m data was closer to matching the ground observations, but categorized the dirt trail as impervious surface. Meanwhile, the Dynamic World 10 m data categorized nearly the entire area as tree cover, with a small corner of impervious surface, entirely missing the trail in the middle, and adding impervious surface where there was none. Finally, the ESRI data showed the entire area as built area, inconsistent with both the other remote sensing sources as well as the ground observations.

At point 27, the ground observation data was not taken directly at the center of the 10000 m² area due to the exact sampling point being located in the middle of the freeway. The ground observations included concrete road and grass and scrub along the side of the road, however due to the off-center location of the ground observation site, CEO classifications were weighed more heavily when comparing land cover with the remote sensing sources. The tree canopy data showed no canopy cover at all, which was consistent with the CEO classifications and ground observations. However, the World Cover 10 m data showed a mix of impervious surface, tree canopy, grassland, and shrubland, in a diagonal pattern that did not match the consistency of the scrub from the CEO classifications. Dynamic World 10 m data showed half of the area to be impervious surface and half shrub and scrub, but compared to the CEO classification that was majority

scrub, this increased impervious surface percentage was also inconsistent. ESRI was similar to Dynamic World 10 m in this area as well, with about half of the area classified as impervious surface and half as rangeland, but in a different pattern than Dynamic World 10 m.

At point 33, the ground observations were taken slightly outside of the 10000 m² area due to obstructive vegetation. However, the observations were representative of the land cover in the area as confirmed visually. Ground observations and CEO classifications showed dense shrub and brush coverage, with small trees. Tree canopy data showed some canopy height but not in any consistent pattern with CEO classifications. World Cover 10 m data was more consistent with the CEO classifications, but included a large corner of impervious surface that was not present in the ground observations or CEO classifications. Dynamic World 10 m data represented nearly the entire area as built up, as did ESRI, both inconsistent with the CEO classifications and ground observations.

25 of the 37 points contained at least partially built-up areas, which were mainly categorized as completely built-up by remote sensing sources despite some human-placed vegetation.

4. Discussion

Overall, land cover data from remote sensing sources were accurate when compared to field observations and manually-categorized CEO data. The Dynamic World 10 m and ESRI 10 m datasets were less detailed than the World Cover 10 m dataset when comparing the land cover classifications between the sources. This comparison is notable due to the identical spatial resolution of the data for Dynamic World, ESRI, and World Cover. While it would be expected that the finer resolution 1 m Tree Canopy data would result in more detail compared to these land cover classification layers, the differences between land cover classification layers of the same spatial resolution were surprising. World Cover 10 m tended to better capture the land cover in detail, such as capturing the trees in a residential area. This led to generalized categorization in built-up areas where Dynamic World and ESRI categorized the entire area as built-up, but in many cases vegetation, tree cover, or other features were clearly present from field observations and shown in World Cover 10 m, and sometimes in the 1 m Tree Canopy data as well. This overgeneralization of built-up areas is evident with Dynamic World 10 m and ESRI when the comparison of the overall percentage of fractional impervious surface for the AOI was calculated. The approximately 30 percentage points of overestimated impervious surface for these two datasets show how the small but numerous overestimates of built-up land led to drastic differences in fractional impervious surface for the 3 km × 3 km area, compared to the authoritative results of the MRLC data. In these cases of overestimation, remote sensing data was correct for parts of, but not the entire, 10000 m² area. As seen from the LTS images starting in 1984, and the MRLC Fractional Impervious Surface images starting in 1985, the AOI has gone from completely undeveloped to almost completely built-up, with shrub-covered canyons remaining the only unchanged areas over forty years. This rapid development has been captured by remote sensing at the majority of the points examined, with the exceptions of the points that are in disagreement. Disagreement points have the opposite issue, where remote sensing data categorizes the area as built-up, however, the area is covered in natural vegetation.

Limitations of this study arise in several forms. First, the time difference between the remote sensing data and the ground observations may be a cause of some inconsistencies. Ground observations were made in the summer of 2025, while remote sensing land cover maps relied on satellite imagery from as early as 2020. In order to consider a range of remote sensing land cover classification layers, the sources were not chosen based on their availability of data from the most recent year, 2024. Given the rapid urbanization of the area, a time span of five years could greatly change the land cover in this area and lead to misleading results. However, as shown in Section 3.1, despite the data from World Cover 10 m relying on imagery from 2021 compared to the more recent Dynamic World 10 m and ESRI data from 2024, World Cover 10 m had a more accurate percentage of impervious surface for the AOI as a whole when all three land cover maps were compared against the MRLC data and CEO observations. Another concern may be the season in which ground observations and CEO classifications were made. The San Diego climate, however, lessens the seasonal difference in vegetation because the climate is moderate and does not vary extremely throughout the year. Vegetation is fairly consistent throughout the year, so while some moderate differences in vegetation due to seasonal changes may be a factor in the differences in land cover observed between remote sensing sources and ground observations, in the specific case of this San Diego AOI, seasonal changes are not as pressing a concern. Finally, interpretation of land cover classification labels is a consideration that must be made. CEO classifications were made with thirteen different labels to choose from, while remote sensing sources had fewer possible labels. For instance, World Cover 10 m has eleven different land cover labels, Dynamic World 10 m has nine labels, and ESRI has nine labels. While many of these labels overlap, most

consistently with "built up" and "trees," the differences in labeling of land cover elements is also something to take into consideration. The question of whether a tree that was planted along a sidewalk and road may be considered to be tree coverage, cultivated vegetation, or considered to be part of the built-up area due to its small size and surrounding impervious surface provides an example of how land cover labels can sometimes be up to interpretation. Given that the remote sensing maps were generated using artificial intelligence or machine learning techniques (Karra et al., 2021; Brown et al., 2022; Tolan et al., 2024), these interpretations are bound to differ between the remote sensing sources and the manual CEO classifications.

5. Conclusions

In relation to the goal of investigating the degree of similarity between field observations and remote sensing data in the AOI, the data show a majority of matches in predominantly built-up areas and predominantly natural areas. About 90% of the 37 points investigated showed agreement between remote sensing data and field observations, based on qualitative visual matches of 34 out of 37 sampling points. As seen with the fractional impervious surface percentages, Dynamic World 10 m and ESRI greatly overestimated built-up areas compared to the authoritative MRLC and CEO data. Consistent with the qualitative findings, the World Cover 10 m land cover layer provides a more detailed and sensitive land cover classification; World Cover 10 m presented a fractional impervious surface percentage within 4 percentage points of the MRLC and CEO data. This estimate of impervious surface was far closer to the MRLC and CEO data than the nearly 30-percentage-point gap from either Dynamic World 10 m or ESRI data. However, the consistency between the CEO and MRLC fractional impervious surface percentages shows that the Adopt a Pixel 3 km strategy provides an accurate assessment of the land cover of a 3 km × 3 km AOI using the 37 points and manual land cover classifications inside 10000 m² boundaries of these points. Remote sensing data can provide a wealth of information, but different sources, as seen in the research, provide differing levels of detail and suitability for specific research objectives. Three of the field observation locations were not within the desired 10000 m² area, and many others were not centered at the desired point, which explains discrepancies between field observations and CEO classifications, both of which are considered reference data. These location differences were caused by limitations such as private property lines and safety in areas of dense vegetation. The photos collected support a successful investigation of land cover categorization similarities and prompt further research on differences among land cover datasets for the AOI over time.

Funding: This research was funded through the NASA STEM Enhancement in the Earth Sciences (SEES) Virtual High School Internship program. The NASA Earth Science Education Collaborative leads Earth Explorers through an award to the Institute for Global Environmental Strategies, Arlington, VA (NASA Award NNX6AE28A). The SEES High School Summer Intern Program is led by the Texas Space Grant Consortium at the University of Texas at Austin (NASA Award NNX16AB89A0).

Data Availability Statement: The annual fractional impervious surface calculations (1985–2024), associated geospatial data, and complete table of sampling point comparisons for this study are available in the Zenodo repository at https://doi.org/10.5281/zenodo.19395850.

Acknowledgment: The authors would like to acknowledge the support of the 2025 Earth System Explorers (ESE) Team, NASA Science Mentors, and ESE peer mentors. NASA STEM Enhancement in the Earth Sciences (SEES) Virtual High School Internship program.

Conflicts of Interest: The authors declare no conflicts of interest. The funders had no role in the design of the study; in the collection, analyses, or interpretation of data; in the writing of the manuscript; or in the decision to publish the results.

References

Braaten, J. (n.d.). *Landsat timeseries explorer* [Web application]. Retrieved July 30, 2025, from https://jstnbraaten.users.earthengine.app/view/landsat-timeseries-explorer#run=false;lon=-122.91966;lat=44.24135;from=06-10;to=09-20;index=NBR;rgb=SWIR1%2FNIR%2FGREEN;chipwidth=4

Brown, C. F., Brumby, S. P., Guzder-Williams, B., Birch, T., Hyde, S. B., Mazzariello, J., Czerwinski, W., Pasquarella, V. J., Haertel, R., Ilyushchenko, S., Schwehr, K., Weisse, M., Stolle, F., Hanson, C., Guinan, O., Moore, R., & Tait, A. M. (2022). Dynamic World, near real-time global 10 m land use land cover mapping. *Scientific Data, 9*, 251. https://doi.org/10.1038/s41597-022-01307-4

Gorelick, N., Hancher, M., Dixon, M., Ilyushchenko, S., Thau, D., & Moore, R. (2017). Google Earth Engine: Planetary-scale geospatial analysis for everyone. *Remote Sensing of Environment, 202*, 18–27. https://doi.org/10.1016/j.rse.2017.06.031

Jin, S., Dewitz, J., Danielson, P., Granneman, B., Costello, C., Smith, K., & Zhu, Z. (2023). National Land Cover Database 2019: A new strategy for creating clean leaf-on and leaf-off Landsat composite images. *Journal of Remote Sensing, 3*, 22. https://doi.org/10.34133/remotesensing.0022

Karra, K., Kontgis, C., Statman-Weil, Z., Mazzariello, J. C., Mathis, M., & Brumby, S. P. (2021). Global land use/land cover with Sentinel-2 and deep learning. In *2021 IEEE International Geoscience and Remote Sensing Symposium (IGARSS)* (pp. 4704–4707). IEEE. https://doi.org/10.1109/IGARSS47720.2021.9553499

Low, R. D., Nelson, P. V., Soeffing, C., Clark, A., & SEES 2020 Mosquito Mappers Research Team. (2021). Adopt a pixel 3 km: A multiscale data set linking remotely sensed land cover imagery with field-based citizen science observation. *Frontiers in Climate, 3*, 658063. https://doi.org/10.3389/fclim.2021.658063

Mapbox. (n.d.). *Mapbox Satellite* [Technical documentation]. Retrieved April 1, 2026, from https://docs.mapbox.com/data/tilesets/reference/mapbox-satellite/#overview

Multi-Resolution Land Characteristics Consortium. (n.d.). *Annual National Land Cover Database (NLCD) fractional impervious surface*. Retrieved July 30, 2025, from https://www.mrlc.gov/

National Aeronautics and Space Administration (NASA). (2025). Global Learning and Observations to Benefit the Environment (GLOBE) Data User Guide, 2025, version 3.0, https://www.globe.gov.

National Oceanic and Atmospheric Administration (NOAA). (2023, May 2). The marine layer. https://www.noaa.gov/jetstream/ocean/marine-layer

Nelson, P. V., Low, R., Kohl, H., Overoye, D., Yang, D., Huang, X., Chellappan, S., Azam, F. B., Carney, R. M., Falk, M., Garriga, J., Schelkin, L., Boger, R., & Schwerin, T. (2024). GLOBE Observer: A case study in advancing Earth system knowledge with AI-powered citizen science. *Citizen Science: Theory and Practice, 9*(1), 33. https://doi.org/10.5334/cstp.747

Saah, D., Johnson, G., Ashmall, B., Tondapu, G., Tenneson, K., Patterson, M., Poortinga, A., Markert, K., Nguyen, H. Q., Aung, K. S., Schlichting, L., Matin, M., Uddin, K., Aryal, R. R., Dilger, J., Ellenburg, W. L., Flores-Anderson, A. I., Wiell, D., Lindquist, E., Goldstein, J., Clinton, N., & Chishtie, F. (2019). Collect Earth: An online tool for systematic reference data collection in land cover and use applications. *Environmental Modelling & Software*, *118*, 166–171. https://doi.org/10.1016/j.envsoft.2019.05.004

Tolan, J., Yang, H.-I., Nosarzewski, B., Couairon, G., Vo, H. V., Brandt, J., Spore, J., Majumdar, S., Haziza, D., Vamaraju, J., Moutakanni, T., Bojanowski, P., Johns, T., White, B., Tiecke, T., & Couprie, C. (2024). Very high resolution canopy height maps from RGB imagery using self-supervised vision transformer and convolutional decoder trained on aerial lidar. *Remote Sensing of Environment, 300*, 113888. https://doi.org/10.1016/j.rse.2023.113888

U.S. Federal Government. (2025). *U.S. Climate Resilience Toolkit climate explorer*. https://crt-climate-explorer.nemac.org/

U.S. Geological Survey. (2024). *Annual NLCD Collection 1 science products* (Version 1.1) [Data set]. U.S. Geological Survey. https://doi.org/10.5066/P94UXNTS

Zanaga, D., Van De Kerchove, R., De Keersmaecker, W., Souverijns, N., Brockmann, C., Quast, R., Wevers, J., Grosu, A., Paccini, A., Vergnaud, S., Cartus, O., Santoro, M., Fritz, S., Georgieva, I., Lesiv, M., Carter, S., Herold, M., Li, L., Tsendbazar, N. E., ... Arino, O. (2021). *ESA WorldCover 10 m 2020 v100* [Data set]. Zenodo. https://doi.org/10.5281/zenodo.5571936